Title

SEGMENTED LAMINAR FLOW AND OTHER MODELS FOR PACKED-BED LONGITUDINAL DISPERSION

Authors

Hennico, Alphonse
Jacques, Gabriel
Vermeulen, Theodore.

Publication Date

1964-11-16

UCRL-10696 Rev., Pt. II

University of California

Ernest O. Lawrence Radiation Laboratory

LONGITUDINAL DISPERSION IN SINGLE-PHASE LIQUID FLOW THROUGH ORDERED AND RANDOM PACKINGS

Berkeley, California

DISCLAIMER

Rept. submitted for presentation in
the 2nd Symposium on Protection
Against Radiations in Space,
Gallenburg, Oct. 12, 1964.

UCRL-10696 Rev., Pt. II

UNIVERSITY OF CALIFORNIA
Lawrence Radiation Laboratory
Berkeley, California

AEC Contract No. W-7405-eng-48

LONGITUDINAL DISPERSION IN SINGLE-PHASE LIQUID FLOW THROUGH ORDERED AND RANDOM PACKINGS

Gabriel L. Jacques, Alphonse Hennico, Joon Sang Moon
and Theodore Vermeulen

November 16, 1964

UCRL-10696 Rev., Pt. II

LONGITUDINAL DISPERSION IN SINGLE-PHASE LIQUID FLOW THROUGH ORDERED AND RANDOM PACKINGS

Gabriel L. Jacques,* Alphonse Hennico,* Joon Sang Moon,**
and Theodore Vermeulen

Lawrence Radiation Laboratory and
Department of Chemical Engineering
University of California
Berkeley, California

*Present address: Institut Français du Pétrole, Rueil-Malmaison, Seine-et-Oise

**Present address: E. I. du Pont de Nemours and Co., Jackson Laboratory, Wilmington, Delaware

LONGITUDINAL DISPERSION IN SINGLE-PHASE LIQUID FLOW THROUGH ORDERED AND RANDOM PACKINGS

Gabriel L. Jacques, Alphonse Hennico, Joon Sang Moon and Theodore Vermeulen

Step-function injection and purging of a salt tracer in water has been used to measure axial dispersion in sphere- and ring-packed columns. The product of packing Péclet number and void fraction is found to be 0.8 to 0.9 at Reynolds numbers corresponding to the turbulent (eddy) flow range, but only 0.20 in the laminar (filamental) range. For spheres, similar results were given for random packing and for ordered arrangements. It is believed that multiparticle dispersion, or "channeling," was largely absent in the present work. The higher laminar-range Péclet number observed by others for gases is perhaps explained by the difference in Schmidt numbers.

A. Introduction

The extent of axial mixing in columnar equipment can most easily be evaluated quantitatively by unsteady-state tracer-injection techniques independently of mass transfer between phases. A tracer amount of a component is injected in a pattern approaching one of several kinds of idealized disturbance, and the concentration history (or "breakthrough curve") of tracer at a fixed distance downstream from the injection point is measured. The characteristics of the experimental breakthrough or response curve may then be compared with the forms predicted by a mathematical

mixing model. The value of the mathematically calculated mixing parameter that gives the best fit to the experimental curve is designated as the value characteristic of the system.

Several different methods of analysis have been used to measure the breakthrough or response curve. These include ionization-current counting of radioactive tracers, electrical conductivity or electrode potential, and absorption of ultraviolet or visible light. Three different forms of input disturbance are commonly used: a sinusoidal variation, a delta or pulse function, and a step function. The present study utilizes the response to an inlet step function. Experimentally this is carried out by flowing a solute-free liquid and a tracer solution successively through a fixed bed, and determining exit concentration as a function of time. Special care must be taken to obtain a sharp uniform step-function at the inlet. As tracer, a solution of $NaNO_3$ is injected into the system, and the breakthrough curve is measured by electrical conductivity.

Previous Studies

Since 1953 several experimental investigations have been made to determine the nature and the magnitude of the axial dispersion mechanisms. In one of the first studies, Danckwerts made several measurements for flow of water through beds of 3/8-in. Raschig-rings.[7] Later, using the response to a sinusoidally varying input, Kramers and Alberta investigated axial dispersion in water flowing through a column packed with 1-cm. Raschig rings, at Reynolds numbers of 100 and 200.[15] Their phase-shift data yielded dispersion coefficients differing by 50 to 100% from the

values based upon amplitude; the discrepancy was attributed to "trapping" in the interior of the rings.

McHenry and Wilhelm have reported axial-dispersion data for gas flowing through a bed packed with 3-mm. spheres.[18] They used a sinusoidal-input signal, and determined values of the axial-dispersion coefficient from the amplitude change. A value of the Péclet number (defined as $U_0 d_p / E$, with U_0 the superficial velocity, d_p the equivalent-volume sphere diameter, and E the superficial axial-dispersion coefficient) equal to about 2 was found in a Reynolds-number range of from 26 to 1000.

Ebach and White reported the results of liquid-phase longitudinal-dispersion studies for beds of glass spheres, Raschig rings, Berl saddles, and Intalox saddles over a Reynolds-number range from 0.1 to 160.[8] They also investigated the influence of viscosity in a column packed with 1-mm. spheres for a flow rate corresponding to a Reynolds number of 0.25 for water. In this flow region a change of viscosity from 0.95 to 27 centipoises did not influence the axial-dispersion-coefficient values. In comparisons between the different packings, the product of Péclet number and void-fraction was found to be nearly constant. In their experiments, both periodic and transient input signals were used, and the detection method was that of light absorption due to a dye tracer in the water stream. Carberry and Bretton[5] employed pulse-injection techniques very similar to those of Ebach and White, and obtained dispersion coefficients at various flowrates in systems of 0.5, 1, 3, and 5-mm. spheres and 2 and 6-mm. Raschig rings, in a 1.5-in.-i.d. column.

Strang and Geankoplis studied axial dispersion through beds of glass beads, porous alumina spheres, and Raschig rings by the frequency-response technique, using 2-naphthol as a tracer.[23] Their investigation, carried out over a relatively short Reynolds-number range in the laminar region, gave results similar to those of Carberry and Bretton and Ebach and White. Cairns and Prausnitz investigated longitudinal-mixing properties for a water stream flowing through a 2-in. column packed with 2.3-mm. glass spheres, over the Reynolds number range of 22 to 4500.[3] A step input was used in their experiments, with $NaNO_3$ solution as the tracer. Jacques and Vermeulen investigated the axial dispersion during flow of water through beds of ceramic spheres, Raschig rings, and Berl saddles.[14] The present work is a continuation of that study, and certain of those results will be included below.

Although these investigations have resulted in many data concerning the axial mixing of liquids in packed beds, serious discrepancies (as pointed out by Hofmann[13]) exist between the results reported for low Reynolds numbers. Further, no study of the influence of viscosity has been found in the literature for Reynolds numbers larger than 0.25.

B. Apparatus

1. General Specifications

Specifications for the experimental equipment were based upon the following objectives for single-phase breakthrough experiments:

(1) To develop the optimum experimental conditions for determining axial-dispersion coefficients. The variables to be

considered were the concentration and proportion of tracer, the direction of injection (top or bottom of the column), and the sharpness of the step input. Electrolytic conductance was selected as the measure of tracer concentration.

(2) To study the influence of viscosity on the axial-dispersion coefficient. Whereas the gas-phase axial dispersivity appears to remain nearly constant over a wide range of Reynolds numbers (for reasons to be discussed later in this article), the liquid phase is believed to show a transition from a "laminar" to a "turbulent" flow regime[5,14] coincident with changes in slope of the friction-factor and mass-transfer j-factor curves.

(3) To investigate the influence of different packing-particle types, size, and arrangements upon axial dispersion, over a range significant for predictions on industrial-scale packed-tower apparatus. Ordered arrangements of sphere packing were included so as to determine the possible occurrence of packing-orientation effects in axial dispersion, and to obtain a controlled variation of packing void-fraction.

Apparatus was designed for study over a wide range of flow rates with various sizes and types of packing, as shown in Fig. 1. Experimental needs led to the following specifications:

(a) Owing to the labor involved in packing a column and in installing conductivity probes and an injection head in any chosen arrangement, a column once packed was kept intact for repeated experiments. Consequently, different column sections were designed and built, corresponding to the different packing arrangements chosen for investigation. For each column the packing was locked

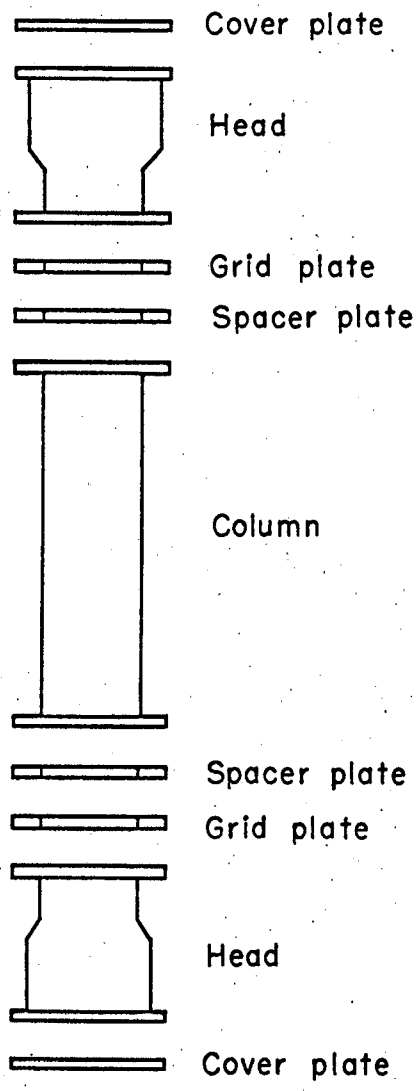

Fig. 1. Exploded diagram of column assembly.

between retaining grids of suitable design. Table I lists the columns and their corresponding specifications.

(b) In order to avoid an expensive duplication of the accessories, everything except the packed column sections was a single installation, while the packed columns were interchangeable. The upper and lower column heads with their accessories (level control, pressure taps, and nozzles) were mounted permanently on the frame in a manner that permitted rapid exchange of the packed sections. A hand-wheel-operated sling supported the head for lifting or lowering, so that one could substitute any of the different column sections. Metallic flexible hoses were connected to the inlet and outlet manifolds for both the top and bottom of the column. The packed sections (weighing approximately 100 lbs.) were transported between the column frame and the storage bench by a hoist supported by an overhead rail.

(c) To meet the flow-rate requirements for one or two main phases plus a tracer stream, a complex assembly of valves, pumps, and rotameters had to be used.

(d) To provide the needed flexibility in breakthrough-curve measurements, conductivity cells in the individual columns were manifolded through switches into a plug connection; this plug was joined by a cable to a recording potentiometer through a second set of switches on the main operating panel.

2. Column Bodies

The adoption of regular as well as random packing arrangements placed many limitations upon the column design. First of all, the triangular and square arrangements chosen necessitated

Table I. Dimensions and packing of experimental columns

olumn umber	Packing	Effective diam (in.)	Equivalent diam (in.)	Arrange-ment	Distance between layer (in.)	Fraction of voids (%)	Column height (in.)	Useful height (in.)	Cross-sectional area(in.^{2})
1	Spheres	0.75	0.75	Tetragonal	0.53	32.0	26.9	23.6	30.3
2	Spheres	0.75	0.75	Ortho-rhombic-1	0.65	38.0	25.8	23.0	30.3
3[a]	Raschig rings	0.25	0.22	Random	0.29	73.0	26.4	26.0	30.7
4[a]	Pellets	0.25	0.23	Random	0.21	35.0	26.4	26.0	30.7
5	Spheres	0.75	0.75	Random	0.71	41.2	26.0	25.0	30.7
6	Spheres	0.75	0.75	Ortho-rhombic-2	0.75	39.5	26.3	24.0	30.6
7	Raschig rings	0.75	0.65	Random	0.88	64.8	26.3	23.6	30.7
8[a]	Intalox saddles	1.0	0.72	Random	0.96	74.0	26.4	26.0	30.7
9[b]	Berl saddles	1.0	0.76	Random	—	68.6	26.4	25.0	30.7
10[b]	Spheres	0.38	0.38	Random	0.35	42.0	26.4	25.0	30.7
11[b]	Spheres (glass)	0.0058	0.0058	Random	0.0055	40.0	26.4	19.0 23.5	30.7

[a] Packing used only by Jacques[14]

[b] Packing used only in the present investigation

[c] Ceramic, except where stated

flat-sided columns; thus, hexagonal and octagonal columns of calculated cross-section were built, in order to simulate as closely as possible a cylindrical symmetry. Considerations of corrosion resistance, minimum weight, cost, and deformation during the needed welding operation led to the choice of aluminum rather than stainless steel for the project. Specifically, 3/16-in. 61ST aluminum sheet (alloyed with 0.25% copper, 0.6% silicon, 1% magnesium, and 0.25% chromium) was used. Cylindrical columns of the same material were built for random packings. Fins were welded on the sides of each column for strengthening and to facilitate handling. Further, the design of each of the grids that locked the packing inside the column had to be selected according to the packing geometry.

The photograph in Fig. 2 shows Column 1 (see Table I), before packing and before drilling for the introduction of conductivity leads and sampling tubes. The bottom grid is attached to the body; the top grid and the corresponding spacer plate are removed. There are two rings of bolts at each end; the inside rings are used for locking the grid to the body, and the outside rings to attach the column to the permanent head and bottom; the four slots in the grid were cut out for the bolts attaching the bottom to the frame. O-rings provided leakproof seals between the flanges. Finally, 3/16-in. reinforcing plates were welded on to provide needed thickness for installation of the sampling outlets. These outlets were placed at nominal distances of 0, 3, 6, 12, and 18 in. from the level of the injection manifold, the spacer plate corresponding to 24 in. The holes in the fins are for insertion of the lifting hoist.

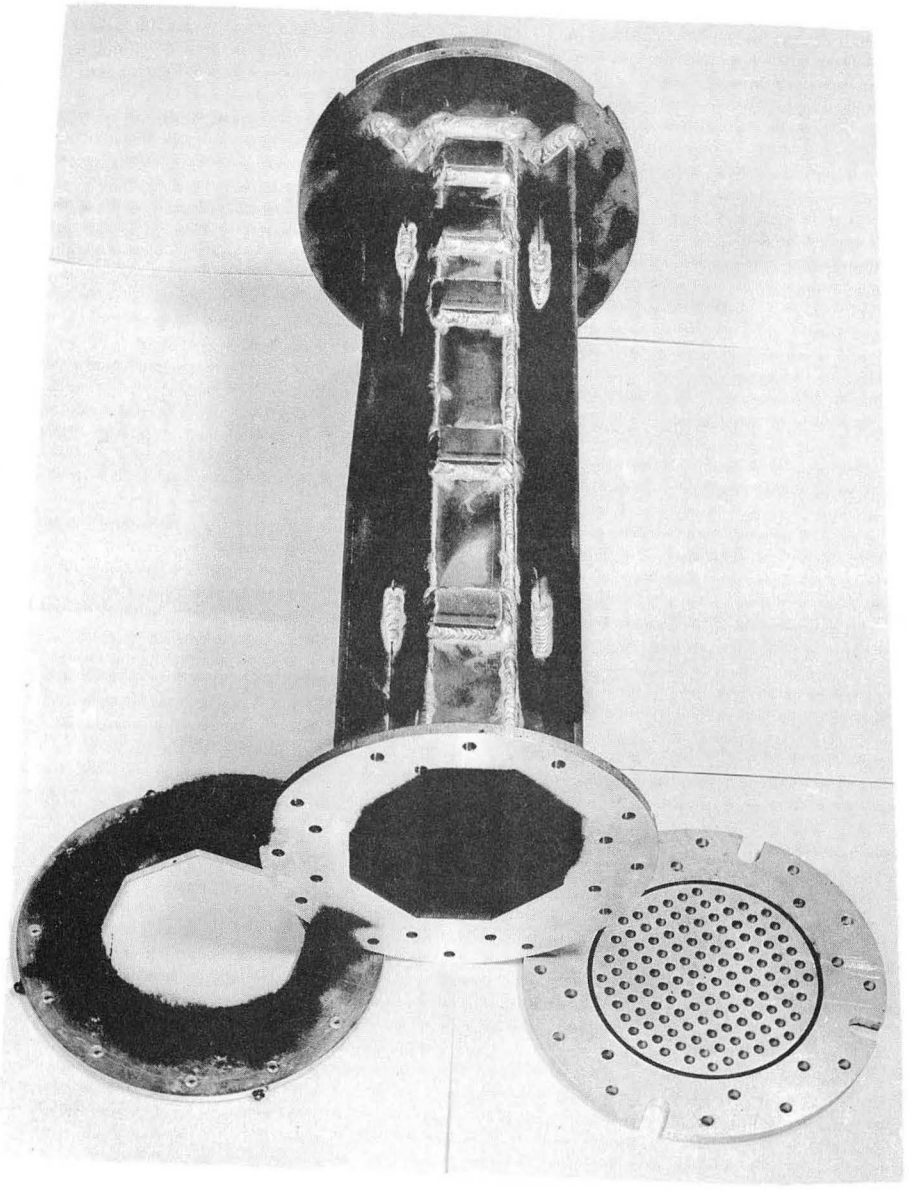

ZN-1818

Fig. 2

3. Column Packing

The ordered arrangements of uniformly-sized spheres correspond to known types of crystallographic lattice. For such arrangements in packed columns, one must select two parallel planes through the lattice that will represent the ends of the column, and several planes each perpendicular to these that will constitute the column walls. The different lattice structures for spheres, each available for columns in one or more orientations, have been reported by Graton and Frazer,[10] and Martin, McCabe, and Monrad.[17]

In the present investigation, three different regular packing arrangements of spheres were used: tetragonal sphenoidal (Column 1), orthorhombic-1 (Column 2), and orthorhombic-2 (Column 6). Spheres 0.75-in. in diameter were obtained as over-sized ceramic balls with rough surfaces. They were wet-ground in a ball mill with granular alundum, and classified between 0.740 and 0.760 inch. Because of the geometry of the ordered packing, a boundary problem arose: as the design called for the spheres in one layer to be tangent to the wall, some of the spheres in the next layer would have to be either omitted or cut. This difficulty was avoided by insertion, in alternate layers, of spacers between the walls and the balls. Wall spacers for the second layer for Column 2 are shown in Fig. 3. (The second layer is drawn in light lines; the first layer in heavy lines.)

Column 1, also equipped with wall spacers, was originally intended to have a rhombohedral arrangement (25.9% voids). It appears to have been packed somewhat loosely, as its measured void-fraction was 32%. If this packing density is uniform, as indicated

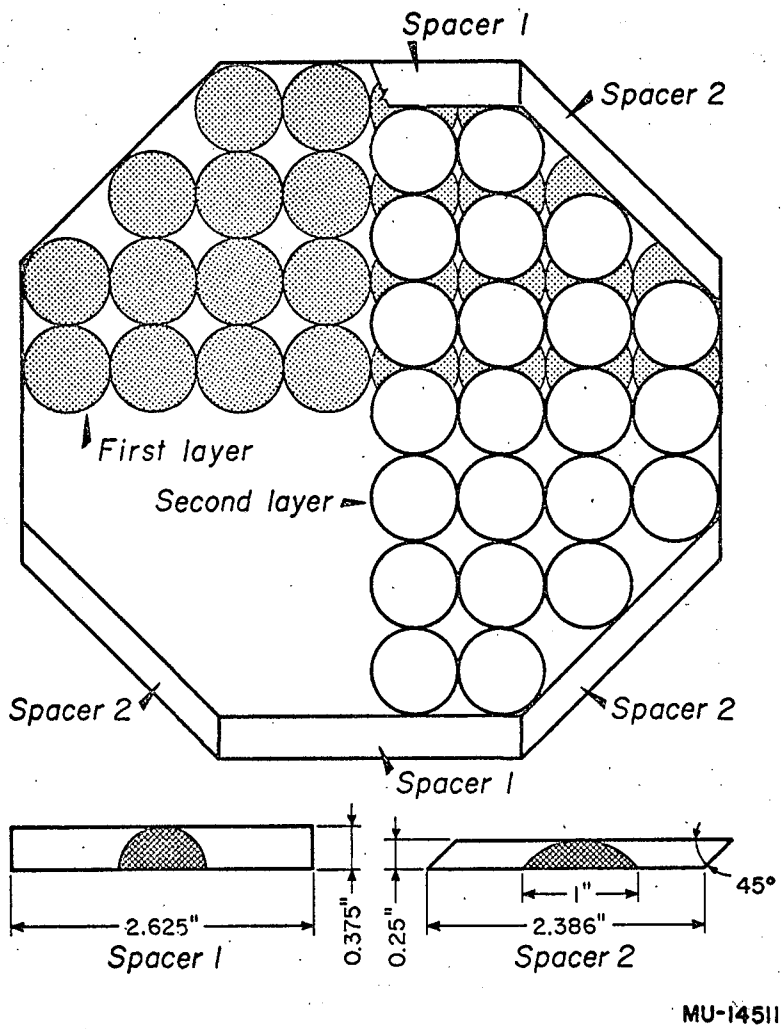

Fig. 3. Arrangement of packing and spacers, column 2 (orthorhombic-1, octagonal).

by the nonoccurrence of shifting when the column is inverted, the packing corresponds to the tetragonal sphenoidal structure;[10,17] hence, this designation is used for Column 1. From Fig. 3, we see that each sphere in the second layer is astride two in the first layer, and that these three spheres form an equilateral triangle perpendicular to the ends of the column. The tetragonal sphenoidal and rhombohedral structures are very similar, with each layer again in a square order, but with the equilateral triangle tilted so that the upper sphere for the former lies more deeply in the hollow center of the square in the first layer. In the tetragonal structure, the angles of tilt (from the vertical) are 30 deg and 26 deg, 34 min; and in the rhombohedral structure, 30 and 30 deg.

The lattice structures of Columns 2 and 6 are identical, but the arrangement of Column 6 is perpendicular to that of Column 2. In Column 6 the triangles are parallel and the squares perpendicular to the ends of the column. Table I gives details on all the types and arrangements of packing used for the investigation.

The randomly packed columns were stacked by pouring the packing into the column with attendant shaking of the bed. They included not only spheres of 0.75-in. and 0.38-in. diameter, but also 0.75-in. and 0.25-in. Raschig rings, 0.25-in. polyethylene pellets, and 1-in. Berl saddles and Intalox saddles.

The void-fraction ϵ was found for all packings by measuring the amount of water necessary to fill a column of known dimensions to a well specified height. The void-fraction of randomly packed spheres is generally close to that for the ordered rhombohedral arrangements. For packings other than spherical balls, several different "equivalent" diameters can be defined.

The most common one is the "equivalent spherical diameter," $(d_p)_v$,[2,16] which corresponds to a sphere having the same volume as the packing unit. Pratt[20] introduced an "equivalent hydraulic diameter," $(d_p)_h$. The diameter of a sphere with the same surface-to-volume ratio as the packing particle, $(d_p)_a$, has also been used.[19] Another property of packed beds is the sphericity (ψ) of the particle. This is defined as the area of a sphere having the same volume as the particle, divided by the area of the particle. We note that $(d_p)_a = \psi(d_p)_v$.

The values used for the above-mentioned parameters in this study are given in Table II.

4. Conductivity Probes

The tracer used was a sodium nitrate solution, with tap water as the main stream; the detection method was that of electrical conductivity. In the concentration range used, the electrical conductance of the aqueous salt solution was proportional to the concentration of the salt. Therefore a knowledge of the conductance of the mixed stream containing the salt tracer allows the direct determination of the concentration behavior in this stream.

The probes used to measure conductivity were constructed of two spherical sectors of 3/4-in. Bakelite balls connected by a pair of rhodium-plated nickel pins, as shown in Fig. 4. They were installed at different heights in the column (nominal 0, 3, 6, 12, 18 and 24 in.) with the plane of the probe being in each case perpendicular to the main direction of the fluid flow. Originally the equipment was also used for the study of radial dispersion, and thus several conductivity probes were installed at different radial positions.[14]

Table II. Packing characteristics

Packing	ϵ	$(d_p)_v$ (in.)	$(d_p)_h$ (in.)	$(d_p)_a$ (in.)	a_p (ft^2/ft^3)	p (ft/ft^2)	ψ
3/4-in. Raschig rings	0.648	0.67	0.47	0.28	80	66	0.42
1-in. Berl saddles	0.686	0.76	0.42	0.25	78	77	0.33
1/4-in. Raschig rings	0.720	0.22	0.16	0.079	240	216	0.36
1-in. Intalox saddles	0.740	0.70	0.40	0.24	78	89	0.34

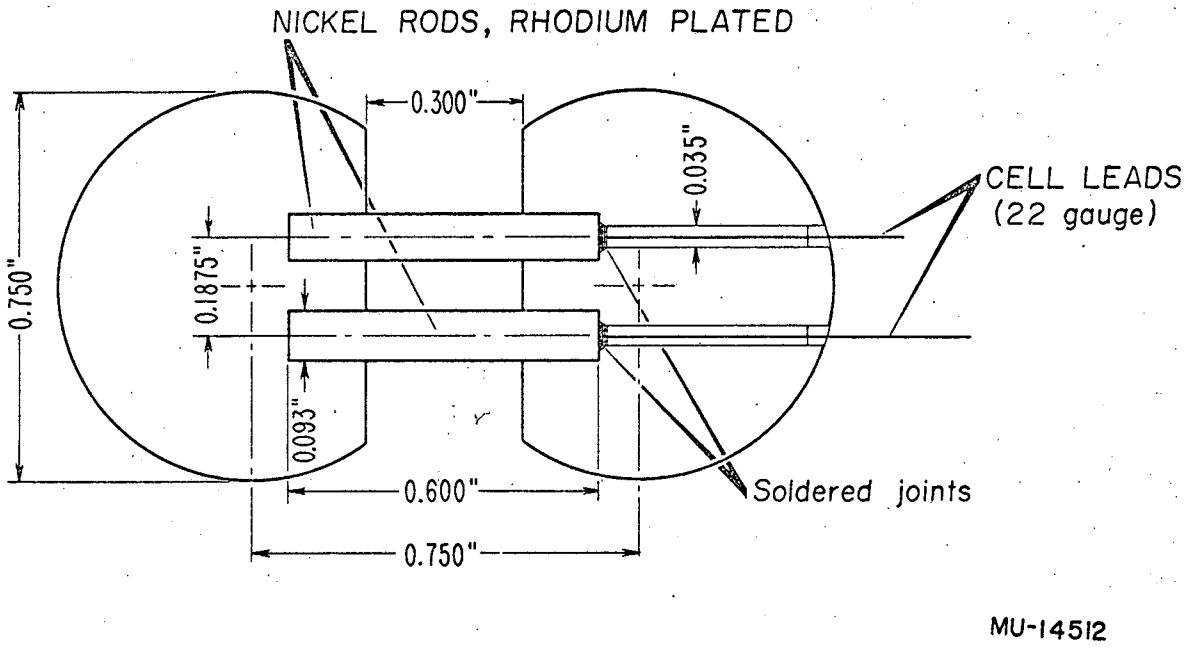

Fig. 4. Construction of conductivity cell.

In the present investigation, only longitudinal dispersion was studied, and only the conductivity probes at the center of the cross-section were selected for use.

5. Injector System

The injection device consisted of several tubes (0.0625-in. o.d., 0.031-in. i.d.) connected to a manifold. At the end of each injection tube an aluminum ball, 3/4 in. in diameter, was affixed. For the central injector, the aluminum ball had 6 holes (0.059-in. diameter) drilled, 60 degrees apart, around a horizontal circle (perpendicular to the injection tube, here vertical). The arrangement and the number of injection tubes (normally, 8) were dependent on the form of the cross-section. The end of each off-center injector was anchored in the bed by being run through a 3/4-in. aluminum sphere. In Column 7, each such aluminum sphere was provided with six outlets.

A small pump continuously recirculated the tracer solution. A 3-way solenoid valve installed near the column allowed a very rapid action for either starting or stopping the flow of the injectant (tracer) into the test section. The pressure drops in the injection path and in the recirculation path were equalized by means of valves in each line adjacent to the solenoid valve.

6. Column Heads

Expanded end sections, identical in construction, were connected above and below the particular packed section in use (Fig. 5). As the columns were designed to operate in both upward and downward flow (see Figs. 1 and 5), the same accessories were adopted for both upper and lower end sections: two windows for

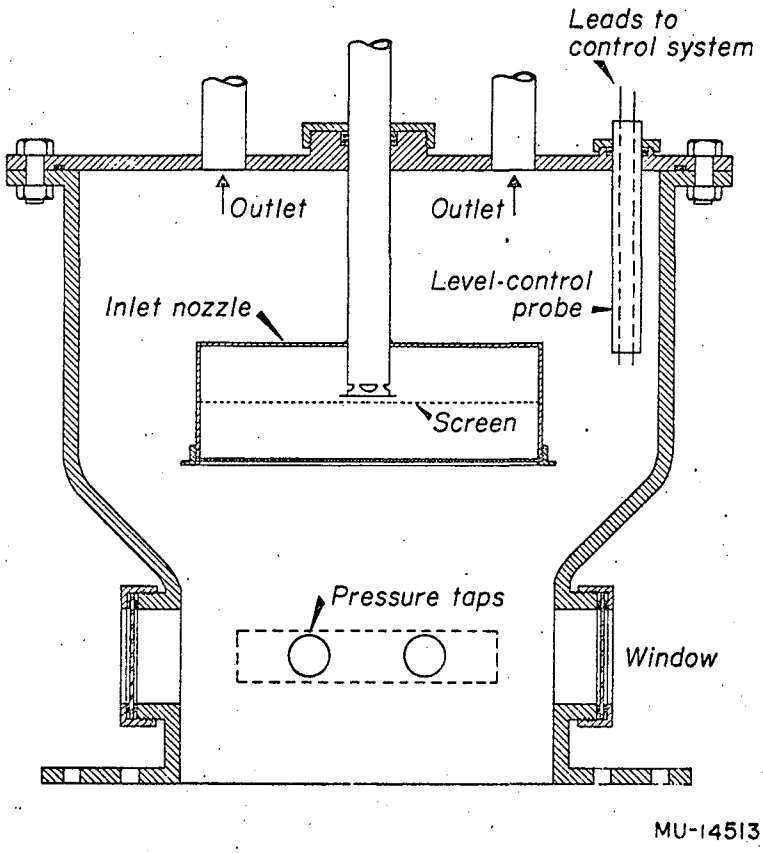

Fig. 5. Diagram of column head.

visual observation, a 6.-in.-diameter inlet nozzle with interchangeable orifice plates designed to give a velocity profile as flat as possible (see Fig. 6), two symmetrically placed outlets, and a liquid-level control probe for subsequent two-phase experiments.

7. Circuitry

The basic electronic circuit used to measure the conductivity consisted of four parts: an amplitude-stable oscillator, a low-impedance voltage source, an amplifier, and a self-balancing potentiometer which feeds the strip-chart recorder. A 1000-cycle oscillator circuit was employed, of bridge "T" type, with thermal nonlinear-element stabilization. The output of the oscillator was fed into a power amplifier consisting of a cathode-coupled phase-inverter driving a push-pull output stage. In series with the probe was a resistor across which a voltage developed, proportional to the current drawn by the probe and thus also proportional to the conductance of the probe. This voltage was amplified and transformer-coupled from a cathode-follower to the detector, whose output was fed to the recorder. Through the use of manual potentiometric span control on the input to the recorder, and of gain controls, a range of conductance from 10^{-5} to 10^{-1} mho could be monitored.

A panel board for wiring was attached to each column body. All the conductivity-cell leads of the column were connected to a rotary switch on the panel, corresponding to up to five combinations of six electrodes. Six double-pole double-throw switches on the column panel allowed the selection of any cell for measurement.

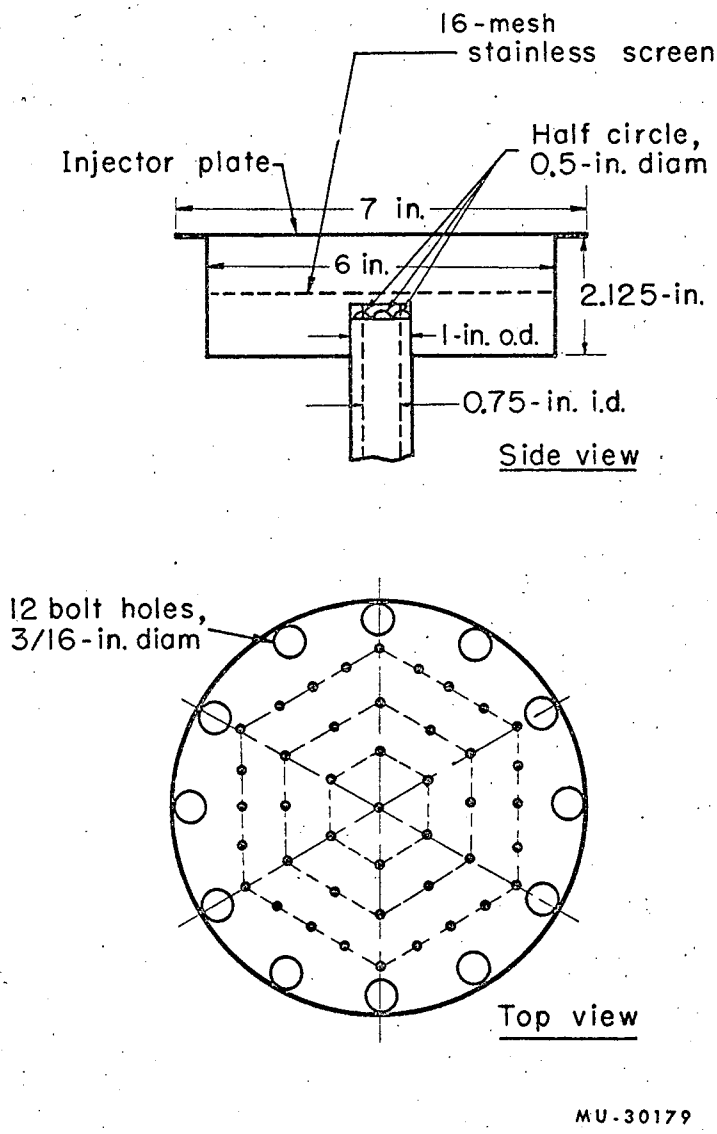

Fig. 6. Detail of nozzle construction.

Finally, an eight-wire-cable plug on the panel board provided a separate connection to the electronic measuring and recording system.

8. Layout and Accessories

As noted in the specifications, the design and construction of a complete pilot-plant unit with extensive manifolding was needed. The flow arrangement is shown in Fig. 7. A set of five pumps, five tanks, and six rotameters made it possible to feed and meter three different types of liquids at the same time for a range of 0.005 gpm to 40 gpm.

Water for the experiments was provided from a 150-gal constant-head tank mounted on the roof of the building, about 25 ft above the column.

The rotameters were each calibrated by weight-flow of water. Flow rates were corrected by assuming that equal-weight flow rates gave equal readings for liquids other than water. The working ranges of water flow through the six rotameters were 0 to 40 gpm, 0 to 6 gpm, 0 to 6 gpm, 0 to 0.8 gpm, 0 to 0.3 gpm, and 0 to 0.005 gpm.

C. Experimental Measurements

1. Determination of Optimum Conditions

The equipment as designed allowed the injection of tracer solution at the top or at the bottom of the column. Theoretically, the same result should be obtained for either injection or shut-off of the tracer for either end of the column; however, it was found experimentally that for low flowrates large differences in behavior could occur. It thus became necessary to find experimentally

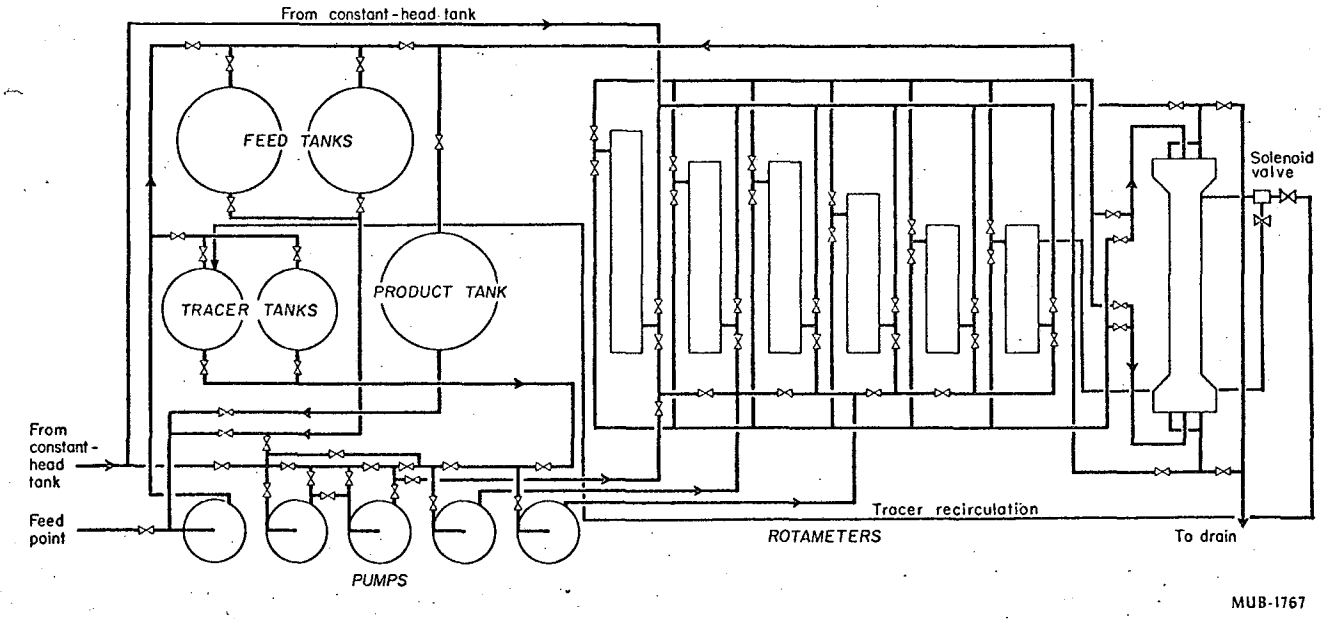

Fig. 7. Layout of flow system.

the operating conditions that would minimize these differences. The smoothness of the breakthrough curve, and the proper correspondence between the calculated and measured stoichiometric times determined in two different ways (that is, by dividing the measured flowrate into the column void volume, and by integrating the experimental breakthrough curve) were also used as criteria for satisfactory operation.

Preliminary studies were therefore made of two columns with different packings: Column 1 (3/4-in. spheres, tetragonal arrangement) and Column 7 (3/4-in. Raschig rings). With water as the main stream, for injection of $NaNO_3$ solution at the top of the column, it was found that the purging curve after the shutting-off of injection gave more uniform breakthrough curves than the start-up of a step input of tracer. For the latter, the empirical stoichiometric point was much higher than the "exact" value. For injection at the bottom the start-up of tracer injection was better.

These experimental findings were believed to be caused by a hydrodynamic instability, resulting from the density difference between the main stream and the tracer solution, which may cause a preferential but irregular downward flow of the denser fluid (or upward flow of the lighter one). Such an effect is well known in displacement processes;[6,12,22,25] the boundary between adjacent dissimilar bands of liquid can become peculiarly distorted by having "fingers" or "channels" of the displacing liquid intrude deeply into the liquid being displaced.

In principle, this gravity effect may be partially or even completely offset by a viscosity effect, although viscosity seems

to have had very little influence in the present study. Displacement by the more viscous liquid favors stability of the boundary, whereas displacement by the less viscous one favors instability. The viscosity effect has been described by Helfferich in the following terms:[12] "Due to packing irregularities, the displacing fluid is the less viscous, the flow resistance in the bulge is smaller, and the flow larger than elsewhere; thus the fingers grow. On the other hand, if the displacing fluid is more viscous than the liquid being displaced, the flow resistance is larger in the bulge than next to it, and thus the channels vanish."

This tendency toward instability could explain why "top-out" and "bottom-in" run conditions give the better breakthrough curves. The curves corresponding to the reverse conditions (indicating unstable behavior) show an unusual breakthrough shape, with a very fast response at the start followed by a very long tail which eventually approaches saturation; such a shape can result from the presence of "fingers."

In our experiments it was also found that by reducing the salt concentration from 1 N to 0.05 N, the shape of the curves was improved, the two stoichiometric times showed better agreement, and a good match was obtained between equivalent tracer-in and tracer-out runs except at flowrates smaller than 0.3 gal/min.

2. Procedure

As a result of the preliminary runs, the following experimental conditions were adopted: For flowrates smaller than 0.5 gal/min, 0.05 N $NaNO_3$ solution was injected at a rate corresponding in all cases to less than 5% in volume (in most cases around 1 to

2%). For higher flowrates, the amount of tracer injected was less than 1% in volume, but the salt concentration was increased to 0.1 N. The injection was made at the top of the column for nearly all experiments. Both injection- and purge-breakthrough curves were recorded; in the low-flowrate region, when the two curves did not agree, data were taken from the tracer-out or purging curves.

The experimental procedure for typical runs was as follows: Preliminary experiments determined the input "span" to the recorder and the amplifier-gain setting for a specified salt injection. The electrical measuring unit was tested for linearity by replacing the conductivity probe by a potentiometer; for all the runs this error was within 1%. The run was started by flowing tap water through the column at a chosen flow rate. The tracer ($NaNO_3$) solution was started through the recirculation line at the appropriate flowrate (usually around 1 to 2 volume-percent of the main stream), and the pressure drops in the injection line and the recirculation line were equalized by means of two manual valves adjoining the solenoid valve.

After a final check of the flowrates, tracer injection into the column was started by opening the solenoid valve, with the starting time for injection marked electrically on the recorder chart. The voltages recorded during each run were proportional to the conductance of the main stream, and thus, as noted previously, proportional to the concentrations of the injected component. Tracer injection was stopped after a constant reading was reached on the chart; the conductivity was again followed as a function of time to give the purging breakthrough curve. The recorder results were then analyzed as explained below.

3. Calculation of Data

From a critical review of the different mixing models,[11] it was concluded that for low flowrates the data would be analyzed both by the random-walk model (which is practically equivalent to the diffusion model with finite boundary conditions) and by the segmented-laminar-flow model with quartic velocity profile. For high flowrates the data would be analyzed solely by the random-walk model.

Output concentrations measured by the recorder were plotted as percentages of the total concentration-increment range, against the logarithm of relative time, t / t_{50}, where the reference time t_{50} corresponds to the 50% concentration point. The experimental breakthrough curve was then compared with theoretical breakthrough curves predicted by the mixing models. This graphical method has the advantage of comparing entire curves, and thus shows whether the theoretical model used is predicting the right overall shape. Once the theoretical models were shown to be applicable, it was found more convenient to compare experimental slopes for different values of column Péclet number N.

For the random-walk model, the dimensionless slope s was converted to a column Péclet number by the relation

$$N = 4\pi s^2 - 0.80 \qquad (1)$$

(The numerical constant is an effective average of derived values, which range from 0.87 at N = 1 to 0.75 in the upper limit.[11]) For the segmented-laminar-flow model, the column Péclet number was obtained from a graph giving the theoretical slopes for different values of N.[10] Finally, the packing Péclet number (P) was found

by multiplying column Péclet number (N) by the ratio of packing diameter to column height (d_p / h).

D. Results and Discussion

The variables affecting axial mixing which were investigated were viscosity, column length, packing characteristics, and liquid velocity. As indicated above, the experimental breakthrough curve can be analyzed either by curve matching on logarithmic-time coordinates, or by taking the midpoint slope on linear t / t_{50} coordinates. Full results as obtained from 60 run conditions (approximately 400 separate breakthrough curves) are given in the original report.[11]

1. Effects of Viscosity and Velocity

To study the effect of varying the viscosity, breakthrough curves were measured in three different packings: Columns 2, 5, and 7. Aqueous solutions of glycerol were used to obtain a kinematic viscosity of 5 to 6 centistokes. In Fig. 8 the results are given and compared with those obtained from pure water (ν = 1.0 centistokes) under the same experimental conditions. All runs were made at ambient temperature, 68 ± 2°F. The figure shows that for the viscosity range considered, there is a definite variation in axial dispersion as the velocity changes. The Péclet number for pure water and for water-glycerol solution are found to be equal for the same Reynolds number.

2. Effects of Packing-Particle Characteristics

Various types of packing were investigated to determine the effects of particle shape and packing arrangement, as listed in

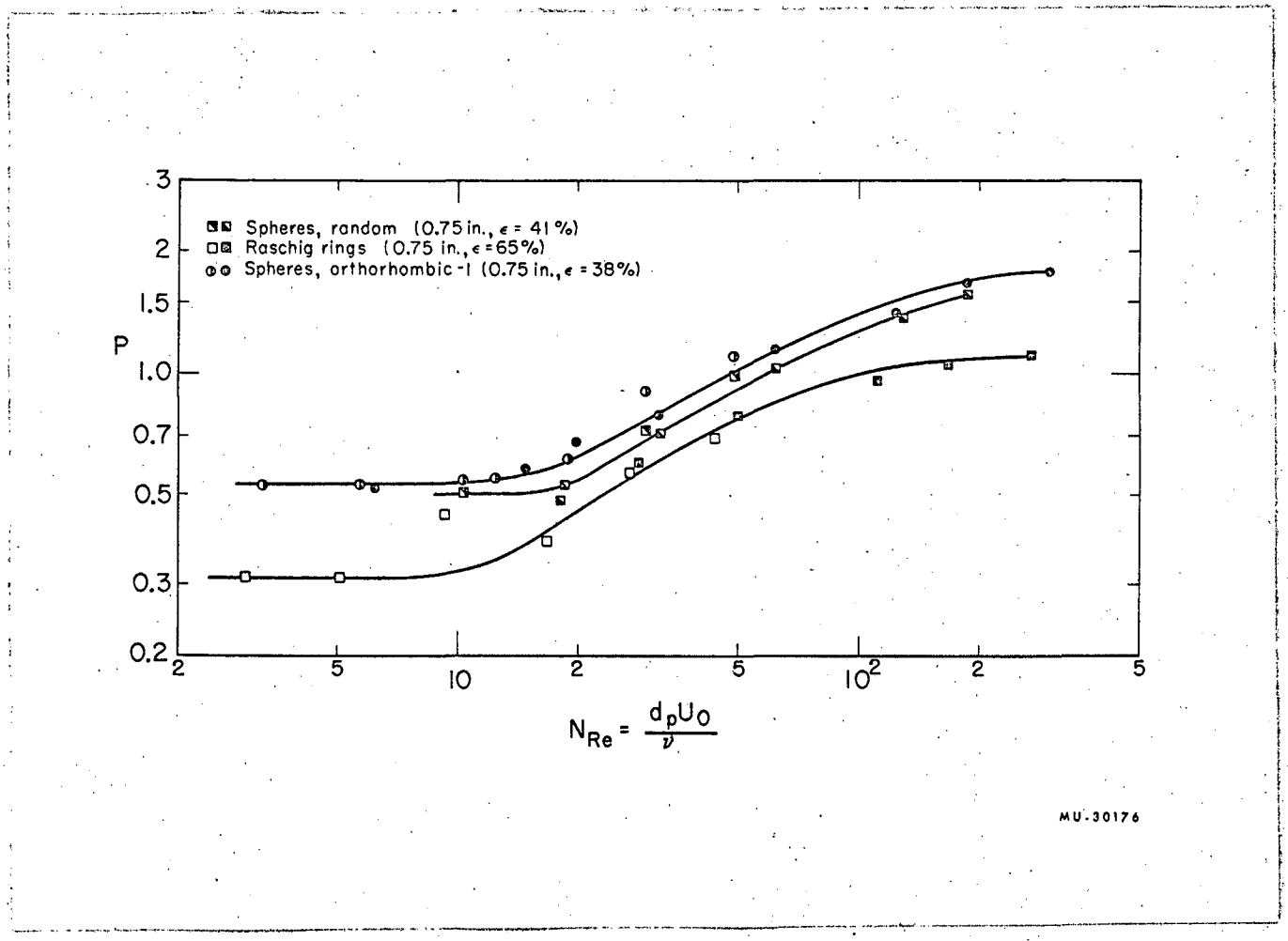

Fig. 8. Influence of viscosity. (In the legend, the symbols on the left are for glycerol-water mixture and those on the right for water alone.)

Tables I and II. Empirical shifting of the plots in Fig. 8 has shown that the points can be consolidated into a single curve, provided the ordinate (Péclet number) is multiplied by the void-fraction ϵ to give

$$\epsilon P \ (= \epsilon \, d_p/\ell)$$

and the abscissa (Reynolds number) is divided by $(1 - \epsilon)$ to give

$$\frac{N_{Re}}{1 - \epsilon} = \frac{U_0 d_p}{(1 - \epsilon)\nu} \qquad (2)$$

where

ϵ = void fraction,

d_p = particle diameter (equivalent spherical diameter for nonspherical particles),

ℓ = mixing length,

U_0 = superficial velocity, and

ν = kinematic viscosity.

The dependence of axial mixing upon the factor $N_{Re}/(1 - \epsilon)$ was adopted from Blake's, Carman's, and Ergun's work on pressure drops in packed beds.[1,4,10] The factor $(1 - \epsilon)$ relates the area per unit volume of particles to the area per unit volume of packed bed. In Ergun's correlation the Reynolds number was not based upon the equivalent spherical diameter, as here, but upon the diameter $(d_p)_a$ of a sphere with the same surface-to-volume ratio as a packing particle. Quite possibly a more complex function of ϵ and of ψ (the sphericity) is involved, which we were not able to develop from data only on high-ψ low-ϵ packings and low-ψ high-ϵ packings.

3. Effect of Bed Length; Choice of Theoretical Model

A crucial factor in determining a longitudinal-dispersion coefficient is the selection of the proper theoretical model for interpreting the experimental data. At least three experimental criteria are available for choosing from among several different theoretical models, in order to determine which model provides the most accurate measure of dispersion behavior. These are:

(1) The shape of the experimental breakthrough curve, in relation to the shapes predicted by the various models.

(2) Related to the shape criterion, the agreement between the observed and the empirical stoichiometric times. (The empirical time is obtained by matching the experimental breakthrough curve to one of a family of theoretical curves, with observation of the point on the actual time scale that matches the stoichiometric point given by the theory.)

(3) Constancy of the Péclet number, or mixing length, for different bed lengths. The different theoretical models all postulate a constant mixing length for the entire packing.

To measure the effect of the bed length, one column unit (Column 10, packed with 0.38-in. ceramic spheres in random arrangement) was used to study breakthrough shapes both at its center (12.-in. level) and at the downstream end. Experiments in this column were conducted at four different flowrates; the results are summarized in Tables III and IV. The values calculated from the random-walk model indicate no effect of bed length, confirming the observations of other investigators;[3,8] whereas the values given by the segmented-laminar-flow model do vary with the bed length.

Table III. Effect of bed length; data analyzed by the random-walk model

Flowrate (gpm)	N_{Re}	N L=23.6 in.	N L=12.0 in.	P L=23.6 in.	P L=12.0 in.
0.3	9.6	36.2	15.5	0.595	0.526
0.5	16.3	36.3	17.3	0.605	0.586
1.0	32.0	46.3	23.4	0.774	0.794
2.0	64.0	61.0	31.4	1.020	1.040

Table IV. Effect of bed length; data analyzed by the segmented-laminar-flow model (quartic)

Flowrate (gpm)	N_{Re}	N L=23.6 in.	N L=12.0 in.	P L=23.6 in.	P L=12.0 in.
0.3	9.6	34.9	8.5	0.576	0.288
0.5	16.3	35.0	10.0	0.579	0.339
1.0	32.0		17.3		0.585
2.0	64.0		29.0		0.980

For experimental runs, usually both models represent the experimental data equally for fractional changes between 0.30 and 0.70; outside this range, the experimental curves lie between the theoretical predictions for segmented laminar flow with a quartic velocity profile and for the random-walk model.

In all cases, the segmented-laminar-flow model showed stoichiometric times about 10% higher, relative to the random-walk and material-balance values. This discrepancy, accompanied by the fact that the Péclet number calculated by segmented laminar flow does depend upon column length, indicates that the random-walk model is somewhat more satisfactory even in the laminar-flow region. At the same time, the segmented-laminar-flow model, based as it is on the filamental nature of laminar flow in packed beds, should be viewed as a necessary step in the development of a better understanding of axial-dispersion phenomena. Its partial failure may well be due to the velocity profile selected, and to the particular methods it involves of averaging the properties of the flow.

4. Graphical Correlation of Results

Using the modified dimensionless parameters just discussed, we have plotted all the experimental points of the present study (on logarithmic coordinates) in Fig. 9. The data clearly show the predicted laminar- and turbulent-flow regimes, with a well-defined transition region occurring, for an $N_{Re}/(1-\epsilon)$ of from 25 to 1000. The data given at high flowrates, for $N_{Re}/(1-\epsilon)$ about 700 (and only these) are from a previous investigation in the same apparatus.[14] The points at abscissas below 1.0 are discussed below.

Fig. 10 shows the data corresponding to the laminar-flow

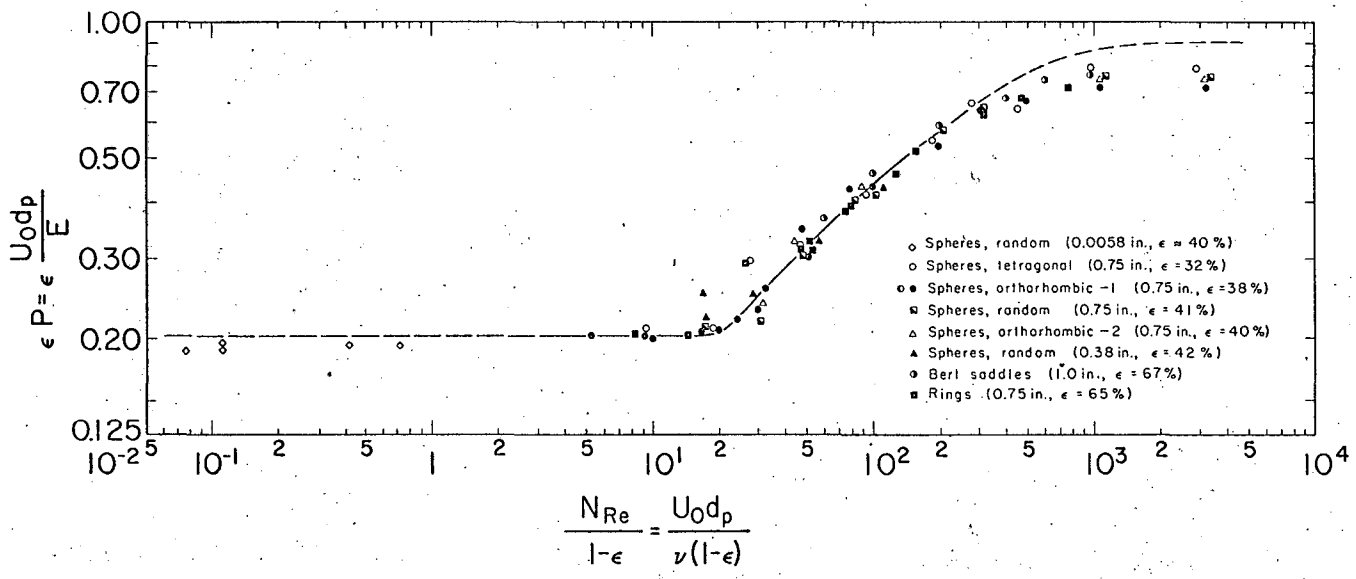

Fig. 9. Experimental results analyzed by random walk.

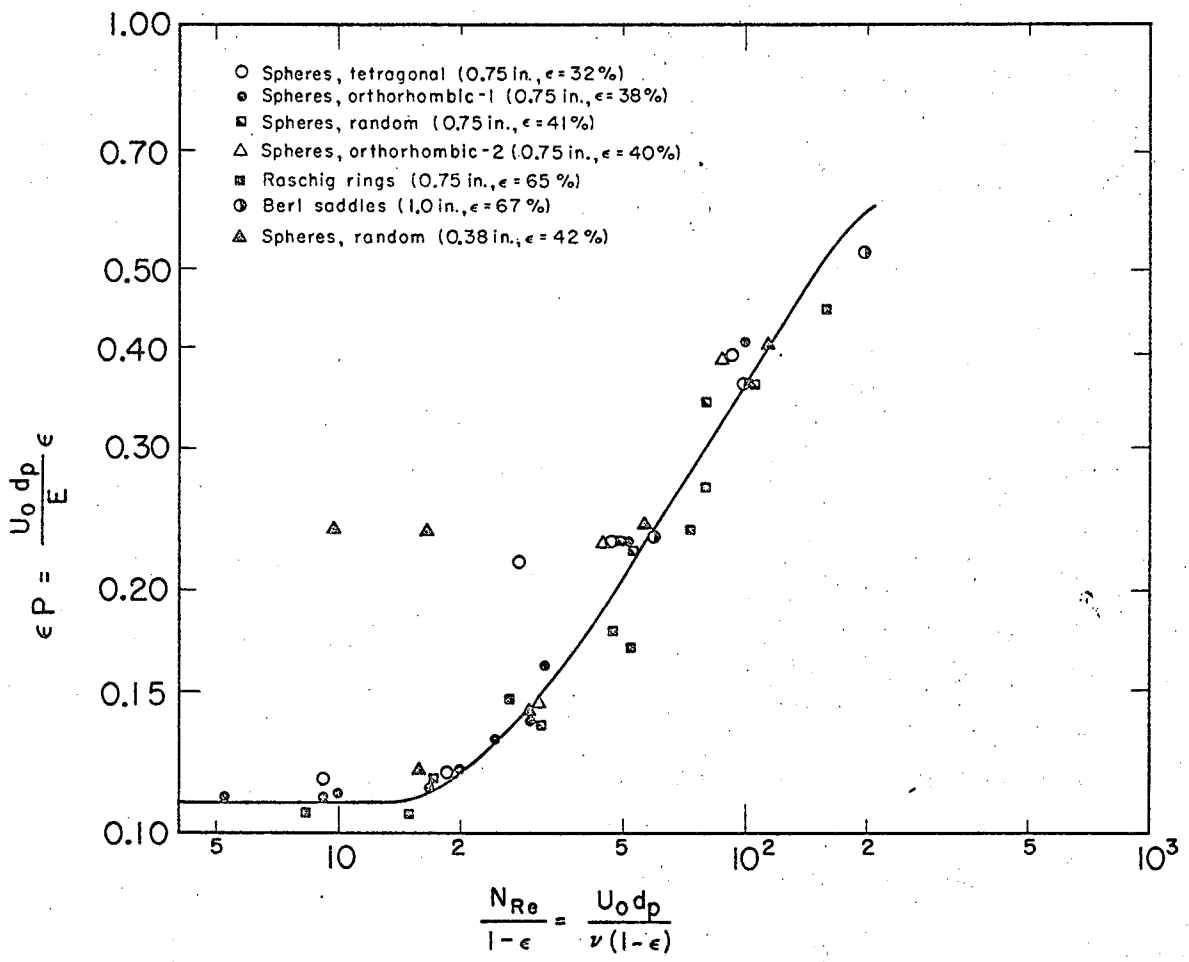

Fig. 10. Experimental results analyzed by segmented laminar flow.

regime and part of the transition region, for a 2-ft column length, analyzed by the segmented-laminar-flow model with a quartic velocity profile. It is seen that the Péclet-number values thus obtained are appreciably smaller at low flowrates than those given by the random-walk model, whereas at higher flowrates they are more nearly equal. As already shown, however, the laminar-flow Péclet values obtained from the segmented-flow model appear to depend upon column length. If points had been shown at different lengths, it would not be possible to represent them by a single curve.

5. Comparison with Other Studies

a. Liquid phase. The experimental results of the present study are compared in Fig. 11 with the data of several earlier investigations. Collectively these data confirm the presence of a transition effect between lower and higher values of Reynolds number. Beyond this general feature, the reproducibility of measurements within any one study seems much better than its agreement with any other one.

Strang and Geankoplis[23] used a sinusoidal input of dye, for 0.23-in. glass spheres and 0.27-in. Raschig rings in a 1.65-in. diameter column 22.5-in. in height.

Jacques's data[14] are from a preliminary study using the presently described apparatus. Subsequent to that study, improvements were made in both the recording and the injection systems, and the tracer-concentration level was greatly reduced.

Cairns and Prausnitz used 0.125-in. glass spheres in a column 2.0 in. in diameter and 24 in. high.[3] A step-function input was selected with upward injection of $NaNO_3$ tracer solution, and

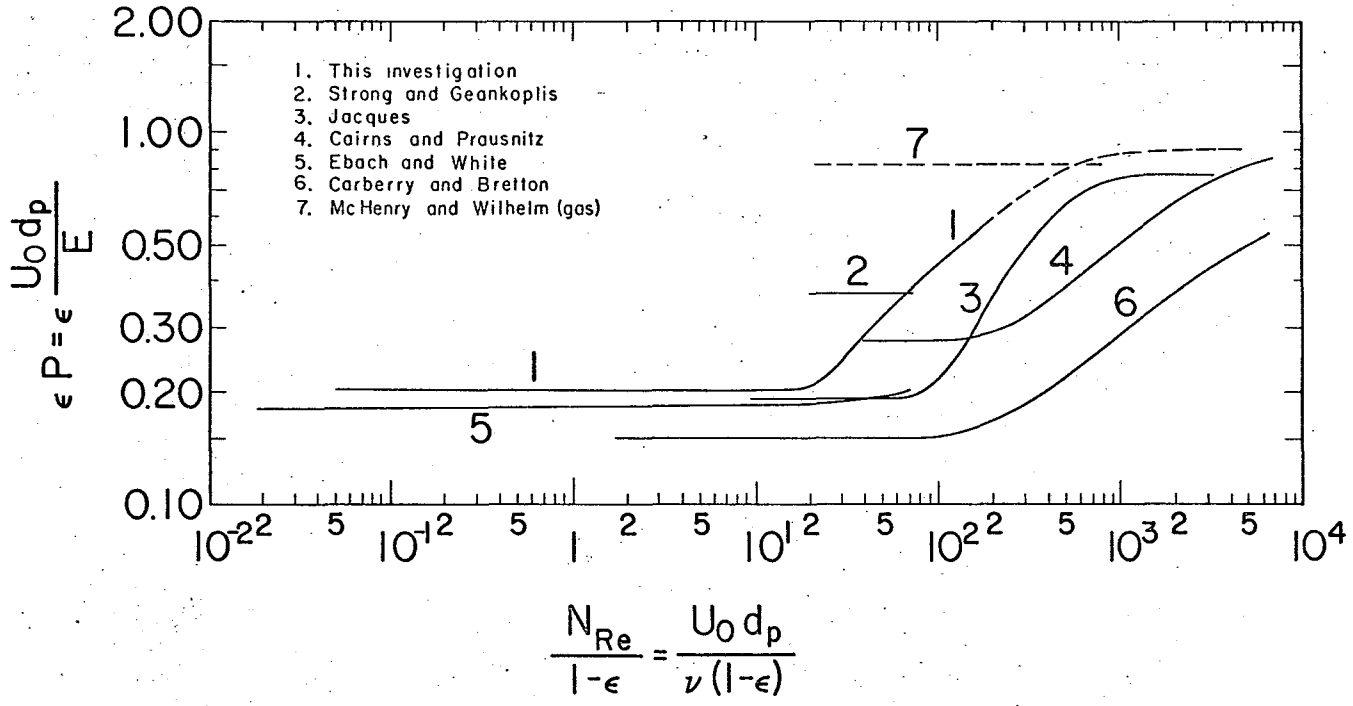

Fig. 11. Comparison with other investigation.

purging-step curves were used for the analysis.

Ebach and White used sinusoidal injection and also pulse injection in a 2.0-in.-diameter column 2.0 to 5.0 ft high, with glass spheres 0.0083, 0.04, 0.13, or 0.27 in. in diameter and 0.25-in. (nominal) Raschig rings, Berl saddles, and Intalox saddles.[8]

Carberry and Bretton used pulse injection of dye tracer in a 1.5-in.-diameter column at various bed lengths, with spheres ranging from 0.02 to 0.20 in. in diameter, 0.08-in. doughnut rings, and 0.25-in. Raschig rings.[5]

To compare these experiments, a number of possible sources of error must be kept in mind:

(1) Hydrodynamic instability
(2) Adsorption of tracer on particle surfaces
(3) Instrument lags
(4) Injection end-effects
(5) Flow irregularities in tracer-injection system
(6) Column wall effect and other channeling

A possibility exists that the correct plotting functions have not yet been found, and that the different curves of Fig. 11 are in better agreement than this plot indicates. However, it would be difficult to reconcile the different results for small glass spheres on any such basis.

The present results were obtained on the largest particles used in any study. Wall effects could have occurred in the randomly packed columns, but not in the ordered ones (Columns 1, 2, and 6). Injection end-effects could occur; but both the close agreement of

the stoichiometric times observed from the input and the output, and the good agreement between 1-ft and 2-ft column lengths, suggest that such end effects are minimal. The possibility of hydrodynamic instability, which clearly interfered with our reproducibility at higher tracer-concentration levels, has been almost entirely excluded by the agreement between injection and purging runs for both upflow and downflow operation.

b. Gas phase. McHenry and Wilhelm have reported the only thorough study of gas-phase longitudinal dispersion in packed beds, with sinusoidal input of hydrogen or ethylene into a nitrogen stream.[18] Their measurements were made with 0.127-in. glass spheres in a column 1.94 in. in diameter, with several different bed heights. With some evidence for a dip at $N'_{Re} = 250$, their data led to a P value of 1.88 ± 0.15 or a ϵP value of 0.73 ± 0.06 over the range of N'_{Re} from 20 to 1000. They, and also Carberry and Bretton,[5] have reported a few values for the fine-particle low-flowrate region. Taken together, these results indicate that the gas-phase Péclet-number values are essentially the same in the turbulent and the laminar regimes, but that at sufficiently low Reynolds numbers molecular diffusion predominates and causes the Péclet number to decline.

As already noted, the liquid-phase values from both this and other investigations tend to join McHenry's gas-phase data in the turbulent region, but then decrease to a level one-fourth to one-third of this value in the laminar region. It appears likely that, in gas-phase laminar flow, lateral molecular diffusion in the void spaces compensates for the segregation due to velocity distribution,

and maintains the individual voids in an almost entirely mixed condition.

Figure 12 has been drawn to examine and illustrate the logical consequences of this assumption. Except for axial molecular diffusion, the range of possible modified Péclet numbers appears to be bounded by a segregated-flow value of 0.205 and a void-cell-mixing value near 0.8. The actual gas-phase behavior is indicated by dashed lines, and the known and postulated liquid behavior is indicated by solid lines.

6. Theory of the Laminar-Flow Liquid-Phase Behavior

G. I. Taylor has shown for laminar flow inside pipes that the segregation of residence times (resulting from the velocity profile) can be represented by an effective axial-dispersion ("Taylor-diffusion") coefficient.[24] As radial dispersion becomes appreciable, it serves to reduce the apparent axial coefficient; for this region, in a tube of diameter d_t, in which the average fluid velocity is U, the longitudinal-dispersion coefficient is E and the molecular-diffusion coefficient is D, Taylor derived the relation

$$\frac{E}{Ud_t} = \frac{1}{192}\frac{Ud_t}{D} \qquad (3)$$

For a column randomly packed with spheres we may assume a "tube" diameter equal to half the particle diameter. Then, with $\epsilon = 0.40$, we have

$$\frac{E}{U_0 d_p} = \frac{1}{123}\frac{d_p U_0}{D}, \qquad (4)$$

where U_0 is the superficial velocity ($= U\epsilon$). Introduction of the dimensionless groups,

$$P' = \epsilon P = \frac{U_0 d_p}{E} , \tag{5}$$

$$N'_{Re} = \frac{N_{Re}}{(1-\epsilon)} = \frac{U_0 d_p}{\nu(1-\epsilon)} , \tag{6}$$

and $N_{Sc} = \nu/D$, provides the relation

$$P' = \frac{205}{N_{Sc} N'_{Re}} . \tag{7}$$

Thus, for any given Schmidt number, reducing the Reynolds number should eventually increase the Péclet number from the lower curve to the upper curve. The lines of constant N_{Sc} rising from right to left correspond to the behavior indicated by Eq. (7). With gases, having $N_{Sc} \approx 1$, the rising curves are intersected almost before the fully turbulent region is departed from (McHenry's curve does show a relatively narrow dip at $N'_{Re} = 250$, of perhaps 15%).

With liquids, the rising curves apparently are not reached within the usual range of chemical engineering measurements, i.e., at N'_{Re} values of 1 and greater. Raimondi et al. used pulse injection of radioactive tracer in a 1.22-in.-diameter column 35.4 in. high, with glass beads 0.0045, 0.0214 and 0.0256 in. in diameter.[21] Their data led to a P value of 1.45 ± 0.2 (or ϵP of 0.575 ± 0.07) over the range of N'_{Re} from 0.015 to 0.28. Although this Péclet number value is lower than the upper limit (or $P' = 0.75$), which might be caused by channeling, it is much higher than the lower limit ($P' \approx 0.2$). This one experimental finding is in favor of the idea that Taylor diffusion can cause a rise in the Péclet number for liquids at $N'_{Re} < 1$. The reason that P values seem not

to exceed the values found by McHenry and Wilhelm may be that the local velocities are always much higher in the channels between the voids than within the voids. Within each void, both axial and transverse molecular diffusion occur at comparable rates, so that the void is reconverted to a near-perfect mixing cell.

At very low flowrates, molecular diffusion in the axial direction becomes predominant. This effect is indicated by the lines of constant N_{Sc} that fall off to the left in Fig. 12. In this region, the effective diffusivity is $D/\sqrt{2}$, the factor $\sqrt{2}$ being commonly adopted as the tortuosity of the bed. The mixing length, or ratio of effective diffusivity to linear velocity, is $(D/\sqrt{2})(\epsilon/U_0)$. Hence the modified Péclet number P' will be given by

$$P'(= \epsilon U_0 d_p / E) = \sqrt{2}\, U_0 d_p / D \quad . \tag{8}$$

The same definitions for N'_{Re} and N_{Sc} as above then give the relation

$$P' = 0.85\, N_{Sc}\, N'_{Re} \quad . \tag{9}$$

The gas-phase data cited above, for low flowrates, fall in the range of molecular-diffusion curves shown here.

A series of supplemental experiments was conducted to measure the Péclet-number behavior in the region of very low flow rates. Use was made of Column 11, packed with 0.0058-inch-diameter glass beads (Minnesota Mining Mfg. Co.) held by 200-mesh stainless-steel screens. As shown in the dotted-line region of Fig. 10, the modified Péclet numbers remained constant at 0.20 ± 0.02, and the predicted rise did not occur down to the lowest Reynolds number studied.

This experimental result casts some doubt upon the foregoing

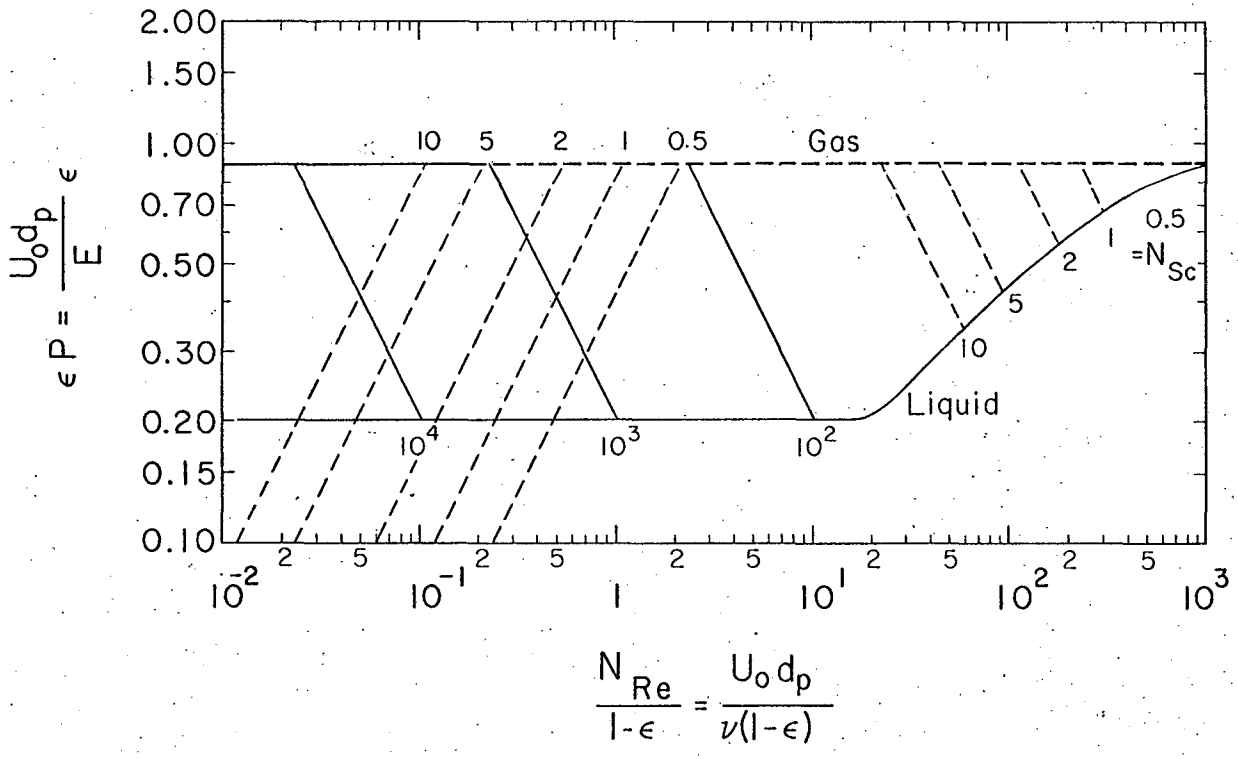

Fig. 12. Postulated relation between liquid- and gas-phase dispersion coefficients.

explanation for the differences in gas and liquid dispersion. Nevertheless it remains possible that the transition postulated to occur at low Reynolds number may in fact depend upon a higher power of Schmidt number due to the nonparabolic velocity distribution. Moreover, recent studies of Green, Perry, and Babcock[10a] indicate that the laminar liquid-phase heat-transfer Péclet number has the higher value characteristic of laminar gas-phase mass transfer; in general, the Prandtl number for liquids has a considerably lower value than the Schmidt number, so that thermal conduction within packing voids should occur more readily than molecular diffusion. Hence Fig. 12 may provide a qualitative, if not entirely quantitative, explanation.

E. Conclusions

The experimental results from this investigation lead to the following conclusions for liquid flow through packed beds:

(a) The data show separate constant values for the Péclet number in the laminar and in the turbulent region, and the existence of a fairly sharp transition curve between these two regions.

(b) The segmented laminar-flow model, derived to provide a physical model for laminar-flow conditions, was found to give a poorer fit to experimental data under such conditions than the random-walk model.

(c) Experiments using water-glycerol solutions indicate that viscosity has a large effect on axial dispersion over the range investigated. The Péclet numbers for pure water and for water-glycerol solutions are found to be equal for the same Reynolds number.

(d) Axial Péclet numbers may be correlated as a function of porosity and of Reynolds number. A plot of modified Péclet

number (ϵP) vs. a modified Reynolds number $N_{Re}/(1-\epsilon)$, shown in Fig. 11, applies to the whole range of experimental results.

(e) No effect of packing arrangement was observed in this study; regular and random packing give identical results for the dame porosity.

(f) An elementary derivation shows that the difference between gas and liquid Péclet numbers (in laminar-flow conditions) can be explained by molecular diffusion in the packing void spaces. However, the rise in liquid-phase Péclet number predicted for values of $N_{Re}/(1-\epsilon)$ between 1 and 10^{-3} has not been observed.

F. Notation

a_p	Surface area per unit volume
c	Concentration
c_0	Concentration for perfect mixing
d_p	Particle diameter
$(d_p)_a$	Equivalent diameter [defined by Eq. (2)]
$(d_p)_h$	Equivalent hydraulic diameter
$(d_p)_v$	Equivalent spherical diameter [defined by Eq. (1)]
d_t	Tube diameter
D	Molecular diffusivity
$\mathscr{D}$	Effective diffusivity within a packed bed
E	Superficial dispersion coefficient
h	Height of bed
ℓ	Mixing length
N	Column Péclet number (h/ℓ)
N_{Sc}	Schmidt number
N_{Re}	Reynolds number
N'_{Re}	Modified Reynolds number $[N_{Re}/(1-\epsilon)]$
p	Periphery of packing
P	Packing Péclet number (d_p/ℓ)
P'	Modified Péclet number (ϵP)
s	Midpoint slope (based on Θ scale)
s'	Midpoint slope of breakthrough curve (based on t/t_{50} scale)
s''	Midpoint slope (equals $[N/(N+1)] \cdot s$)
t	Time
t_{50}	Time corresponding to X equals 0.5
T	Dimensionless time
U	Intersticial velocity or mean linear velocity
U_0	Superficial velocity, equals $U\epsilon$
X	Dimensionless concentration (c/c_0)

β Correction factor to N calculation based on midpoint slope

ϵ Bed void-fraction

Θ Dimensionless time T/N

ν Kinematic viscosity

ψ Sphericity

References

1. F. C. Blake, Trans. Am. Inst. Chem. Engrs. 14, 415 (1922); cited by P. Eisenblau, in Cremer and Davies, "Chemical Engineering Practice," vol. 2 (Butterworths, London, 1946), p. 342.
2. G. G. Brown and Associates, "Unit Operations (John Wiley and Sons, Inc., New York, 1950), p. 216.
3. E. J. Cairns and J. M. Prausnitz, Chem. Eng. Sci. 12, 20 (1960).
4. P. C. Carman, Trans. Inst. Chem. Engrs. (London) 15, 150 (1937).
5. J. J. Carberry and R. H. Bretton, A.I.Ch.E. Journal 4, 367 (1958).
6. R. L. Chuoke, P. Van Meurs, and C. van der Pool, J. Petrol. Technol., Petroleum Trans. AIME 216, 188 (1959).
7. P. V. Danckwerts, Chem. Eng. Sci. 2, 1 (1953).
8. E. A. Ebach and R. R. White, A.I.Ch.E. Journal 4, 161 (1958).
9. S. Ergun, Chem. Eng. Progr. 48, 89 (1952); Ind. Eng. Chem. 47, 1135 (1955).
10. L. C. Graton and H. J. Frazer, J. Geol. 43, 785, 910 (1935).

10a. D. W. Green, R. H. Perry, and R. E. Babcock, A.I.Ch.E. Journal 10, 645 (1964).

11. A. Hennico, G. L. Jacques, and T. Vermeulen, Lawrence Radiation Laboratory Report UCRL-10696, 1963; paper submitted.
12. F. Helfferich, Chem.-Ing. Techn. 34, 275 (1962).
13. H. Hofmann, Chem. Eng. Sci. 14, 193 (1961).
14. G. L. Jacques, J. E. Cotter, and T. Vermeulen, Lawrence Radiation Laboratory Report UCRL-8658, 1959.
15. H. Kramers and G. Alberta, Chem. Eng. Sci. 2, 173 (1953).
16. M. Leva,"Tower Packing and Packed Tower Design," United States

17. J. J. Martin, W. W. McCabe, and C. C. Monrad, Chem. Eng. Progr. 47, 91 (1951).

18. K. W. McHenry and R. H. Wilhelm, A.I.Ch.E. Journal 3, 83 (1957).

19. J. H. Perry, "Chemical Engineers' Handbook," 3rd ed. (McGraw-Hill Book Company, Inc., New York, 1950), p. 394.

20. H. R. C. Pratt, Trans. Inst. Chem. Engrs. (London) 29, 195 (1951).

21. P. Raimondi, G. H. F. Gardner, and C. B. Petrick, "Mixing of Miscible Liquids Flowing in Porous Media," Technical Report from Gulf Research and Development Co., Pittsburgh, Pa., Aug. 31, 1960 (unpublished).

22. P. G. Saffman and G. I. Taylor, Proc. Roy. Soc. (London) A245, 312 (1959).

23. D. A. Strang and C. J. Geankoplis, Ind. Eng. Chem. 50, 1305 (1958).

24. G. I. Taylor, Proc. Roy. Soc. (London) A219, 186 (1953); A223, 446 (1954); A225, 473 (1954).

25. G. I. Taylor, Proc. Roy. Soc. (London) A201, 192 (1950).